A new melting layer detection algorithm that combines polarimetric radar-based detection with thermodynamic output from numerical models

Terry J. Schuur[1,2], Alexander V. Ryzhkov[1,2], and John Krause[1,2]

[1]*Cooperative Institute for Mesoscale Meteorological Studies, University of Oklahoma, Norman, Oklahoma, USA*
[2]*NOAA/OAR/National Severe Storms Laboratory, Norman, Oklahoma, USA*

1 Introduction

The classification of cold-season precipitation at the surface is complicated by the broad range of hydrometeor types that might result from thermodynamic and microphysical processes that occur below the height of the radar's lowest elevation sweep. Because of this, the fuzzy-logic-based hydrometeor classification algorithm that was deployed on the WSR-88D network (Park et al., 2009), which gives classifications on conical surfaces, often provides results in transitional winter weather events that are not representative of the precipitation type observed at ground level. In response to this deficiency, Schuur et al. (2012) reported on initial work to create an algorithm that combines thermodynamic output from a numerical model with polarimetric radar data to produce a *surface-based* classification. The most recent version of this algorithm, which has evolved into an "all-season" algorithm that also takes advantage (under certain warm- and cold-season conditions) of results from the fuzzy-logic-based scheme, is summarized in a separate paper at this conference by Schuur et al. (2014). In short, the transitional winter weather component of the algorithm relies upon the use of thermodynamic output from the High-Resolution Rapid-Refresh (HRRR) model to generate a background classification that is then either accepted or rejected based on observational evidence (determined through an examination of the polarimetric radar data) of the presence/absence of a melting layer (ML). As such, the algorithm's performance relies heavily upon the accurate detection of whether or not a ML exists aloft. This in itself can present challenge since several different methods for detecting the ML exist, with all of them having their own advantages and disadvantages.

The ML detection algorithm that is currently deployed on the WSR-88D network (referred to as the WSR-88D MLDA, Giangrande et al. 2008) uses thresholds of radar reflectivity (Z), differential reflectivity (Z_{DR}), and correlation coefficient (ρ_{HV}) collected at high elevation scans (4-10º elevation) to determine the ML top and bottom at locations close to the radar. However, the algorithm then assumes that the near-radar MLDA detections can be projected out to more distant ranges along each azimuth. This feature has proven to be unrealistic for most meteorological situations, frequently resulting in the extension of a ML into regions where one does not exist. More recently, Krause et al. (2013) presented a technique that uses polarimetric radar data at lower elevation angles (<4º elevation). While the Krause et al. method, which was developed primarily to determine where polarimetric rainfall estimation might suffer from ML contamination, has the advantage of being able to provide ML designations at more distant ranges than is possible with the higher elevations used by the MLDA, the interpretation of the results is often complicated by the effects of beam broadening. Combined, these complicating factors with the radar-based algorithms point to a need for a ML detection method that 1) takes account of the advantages and disadvantages of existing algorithms, 2) can be applied over the entire radar domain, and 3) capitalizes on additional information provided by thermodynamic output from numerical models.

In this paper, we describe a new ML detection algorithm that combines radar observations with thermodynamic output from the HRRR model to provide a "hybrid" ML designation over the entire radar domain. Radar-based, range-dependent Gaussian weighting functions for both high- and low-elevation ML designations, which take into account inherent errors known to each technique, are combined with a model-based Gaussian weighting function that depends on horizontal gradients in wet-bulb temperatures to create a "blended" map of ML detections. A separate, time-dependent weighting function is used to account for time lag in the model analyses by de-emphasizing the contribution from the numerical model as the Δt from the radar volume and the most recent model analysis becomes large.

2 Methodology

The blended ML is created through the combination of output from three distinct melting layer detection techniques: 1) the ML detection algorithm of Giangrande et al. (2008), which uses polarimetric radar data from 4-10º elevation scans, 2) the ML contamination product of Krause et al. (2013), which uses polarimetric radar data from scans < 4º elevation, and 3) the region of ML, here defined as a wet bulb temperature (T_w) of 0ºC < T_w < 4ºC, that is output from the HRRR model. In the following discussion, we use the subscript "h" to refer to the Giangrande et al. (2008) ML product since it was derived from higher elevation scans, the subscript "l" to refer to the Krause et al. (2013) ML product since it was derived from lower elevation scans, and the subscript "m" to refer to the ML as determined from the numerical model output.

The first step in the combination process is to determine which ML detection methods indicate the presence of a ML at each individual gate. For any individual radar ray at a given azimuth and elevation (< 4°), we assign three indices (I_m, I_h, and

I_l) to a each range gate along the ray. $I_m = 1$ if the HRRR T_w at the gate is between 0 and 4°C, otherwise $I_m = 0$. $I_l = 1$ if the gate falls into the ML contamination area as determined by Krause et al. (2013), otherwise, $I_l = 0$. Similarly, $I_h = 1$ if the gate falls into the ML contamination area as determined by Giangrande et al. (2008), otherwise, $I_h = 0$. Since the existing ML detection algorithm (Giangrande et al. 2008) produces two numbers for a given azimuthal direction: H_b and H_t corresponding to the heights of the bottom and top of the melting layer. The geometrical projections of H_b and H_t on the radar ray delineate the segment of the ray where $I_h = 1$ and $I_h = 0$ outside of the segment. The gates with I_h, I_l, and I_m equal to 1 are generally different as illustrated in Fig. 1.

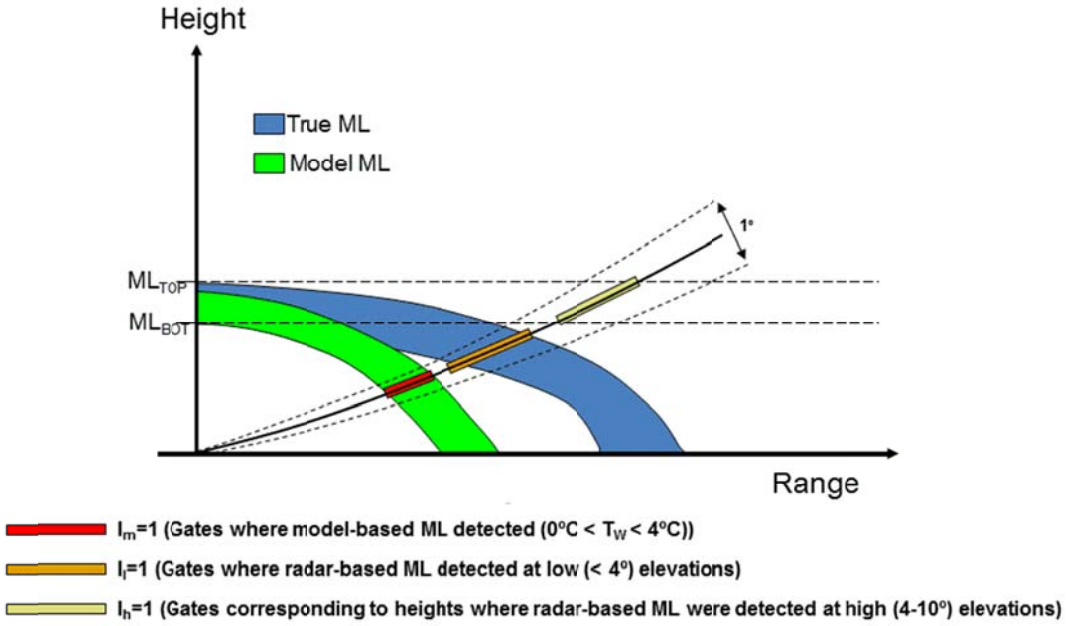

Figure 1: Melting layer designation at lower antenna elevations.

The segments that indicate melting layer for each product are then combined into a single melting layer product by computing an aggregate weight between 0 and 1, where:

$$A = \frac{W_t W_m I_m + W_l I_l + W_h I_h}{W_t W_m + W_l + W_h} \tag{1}$$

W_m, W_l, and W_h are Guassian weights associated with the three products, where the weights are determined as follows

$$W_m = 0.5 \exp\left(-0.69 \frac{g^2}{g_0^2}\right) \tag{2}$$

$$W_l = f_l(r) \exp\left(-0.69 \frac{r^2}{r_{0l}^2}\right) \tag{3}$$

$$W_h = f_h(H_b) \exp\left(-0.69 \frac{r^2}{r_{0h}^2}\right) \quad . \tag{4}$$

In (2) – (4), r is a slant range and the variable g^2 characterizes horizontal gradients of T_w at the height $H_0 = 1.5$ km

$$g^2 = \left(\frac{dT_w(H_0)}{dx}\right)^2 + \left(\frac{dT_w(H_0)}{dy}\right)^2 \tag{5}$$

Finally, we introduce,

$$W_t = \exp\left(-0.69 \frac{t^2}{t_0^{\,2}}\right) \tag{6}$$

where W_t is a time-dependent weighting function that is used to account for time lag in the model analyses by de-emphasizing the contribution from the numerical model as the Δt from the radar volume and the most recent model analysis becomes large.

The parameters g_0, $r_{0l,}$ and r_{0h} are adaptable and will continue to be optimized in the process of testing the algorithm. In this paper, g_0, $r_{0l,}$ r_{0h} and $t_{0,}$ are 0.03K/km, 100 km, 50 km, and 60 min respectively. The factor f_l is equal to 1 for $r > r_{gc}$ and it linearly decreases from 1 to 0 for $r < r_{gc}$ where r_{gc} is the distance up to which the impact of ground clutter (gc) contamination on the quality of the product "l" can be significant. For most radars, setting r_{gc} to 30 km seems to be reasonable. The purpose of introducing factor f_l is to reflect the fact that the quality of the "l" product might be compromised in the presence of ground clutter. Similarly, the factor f_h is introduced to account for degradation of the "h" product at very low melting layer (or low H_b). Hence, $f_h = 1$ if $H_b > h_{gc}$ and f_h linearly decreases to 0 for $H_b < h_{gc.}$ For this study, h_{gc} is 1.0 km.

The expression (1) for the aggregation value A is constructed in such a way that A varies between 0 and 1. If a given range gate is classified as ML by all three ML products then A = 1. If the aggregation value is above certain threshold A_0 (we may start from $A_0 = 0.5$) then the gate is classified as "true" ML. Note that if the wet bulb temperature field is uniform and g = 0 then $W_m = 0.5$ over the whole radar coverage area regardless of the distance from the radar. The range-dependent weights W_l and W_h are higher than W_m at closer distances and lower than W_m far away from the radar.

Fig. 2 illustrates how the decision about the presence of the ML aloft might be made based on the results of "true" ML designation at antenna elevations less than 4°. According to the suggested approach, there is no need to examine a vertical column in order to identify ML aloft. Instead, all ML points identified at lower conical scans are mapped to the surface. A pure model designation is performed at longer distances where the lowest tilt overshoots the melting layer. At close proximity of the radar before the closest ML point identified via the combination of "m", "l", and "h", the choice should be made based on the "m" and "h" designations using the aggregation value

$$A = \frac{W_t W_m I_m + W_h I_h}{W_t W_m + W_h} \quad . \tag{7}$$

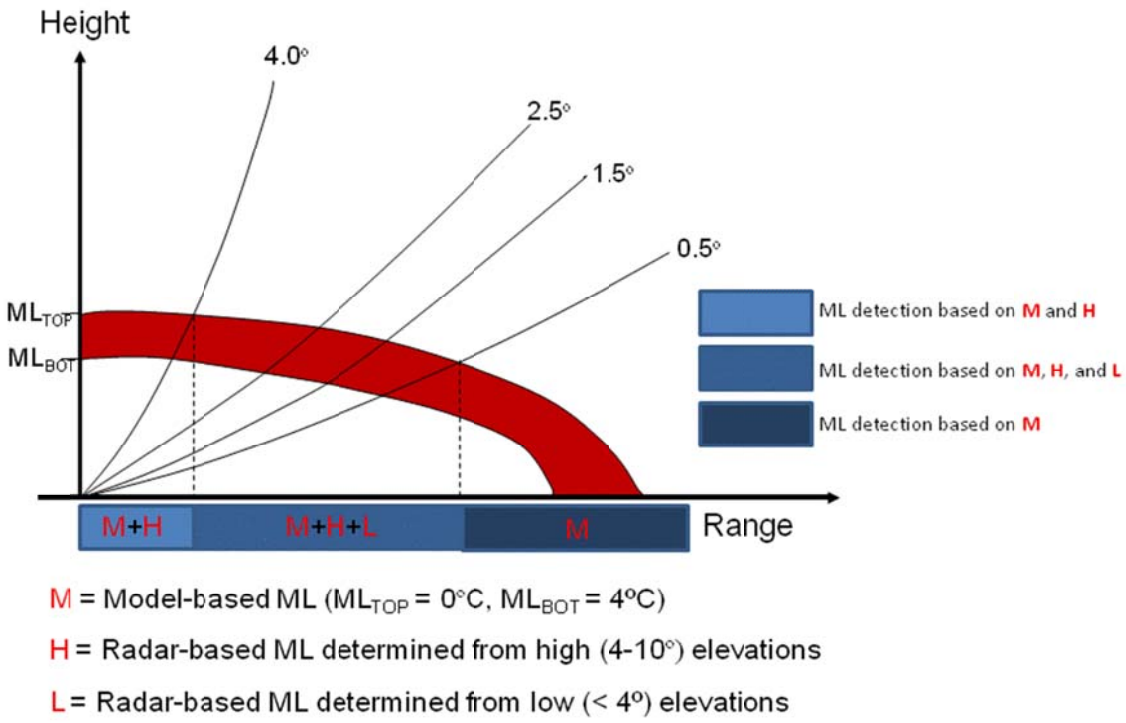

Figure 2: Schematic showing contributions, with range, of each method of ML detection to the overall hybrid product.

3 Example – Northeastern U.S. Blizzard of 8 February 2013

On 8 February 2013, the Northeastern U.S. experienced a historic winter storm that resulted in snow accumulations up to 100 cm in depth. Figure 3, at 2216 UTC on 8 February 2013, shows Z, Z_{DR}, and ρ_{HV} from the KOKX (New York City National Weather Service Office, located on Long Island at Upton, NY) WSR-88D radar. From an examination of the Z_{DR} and ρ_{HV} fields, it is clear that a widespread region layer of warm air was located to the south of Long Island at this time, with the transition from warm- to cold-season precipitation taking place along a region that spanned the entire length of the island. Precipitation type reports during this event supported this transition with widespread reports of rain on the south side of the island and snow (and occasional reports of sleet) to the north. We use this date/time to illustrate the classification procedures followed by the proposed "hybrid" ML detection algorithm.

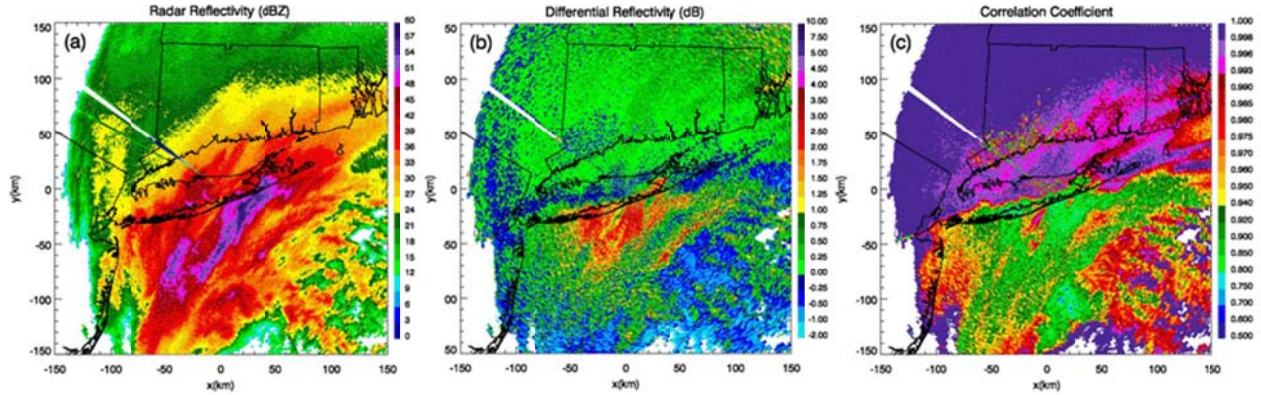

Figure 3: (a) Radar reflectivity (dBZ), (b) differential reflectivity (dB), and (c) correlation coefficient from the KOKX (Upton, NY) WSR-88D radar at 2216 UTC on 8 February 2013.

Figure 4 shows the weights used by the hybrid ML algorithm at this time, where W_m is derived from the HRRR data at H_0=1.5 km using equation (2), W_l is derived from equation (3), and W_h is derived from equation (4). As can be seen from an inspection of Figure 4, W_h drops quickly at relatively short distances from the radar. While ML detection at high elevation angles has been shown through comparisons to sounding data to be highly accurate (Giangrande et al. 2008), the assumed projection of those ML designations to more distant ranges has been found, for many events, to be unrealistic. A sharp reduction of W_h with range therefore works to effectively enhance the contribution from the method at close ranges, but quickly reduce its contribution to the overall product at more distant ranges. In a similar manner, the weights for W_l effectively eliminate it from being a significant contributor at close ranges (where ground clutter may result in false detections), enhance its contribution at intermediate ranges, and then quickly reduce its contribution at more distant ranges where substantial beam broadening can affect the quality of the data. As noted earlier, the weights for all 3 methods (model, high elevation radar-based detection, and low elevation radar-based detection) are controlled through adaptable parameters. At this time, these parameters have yet to be extensively tested.

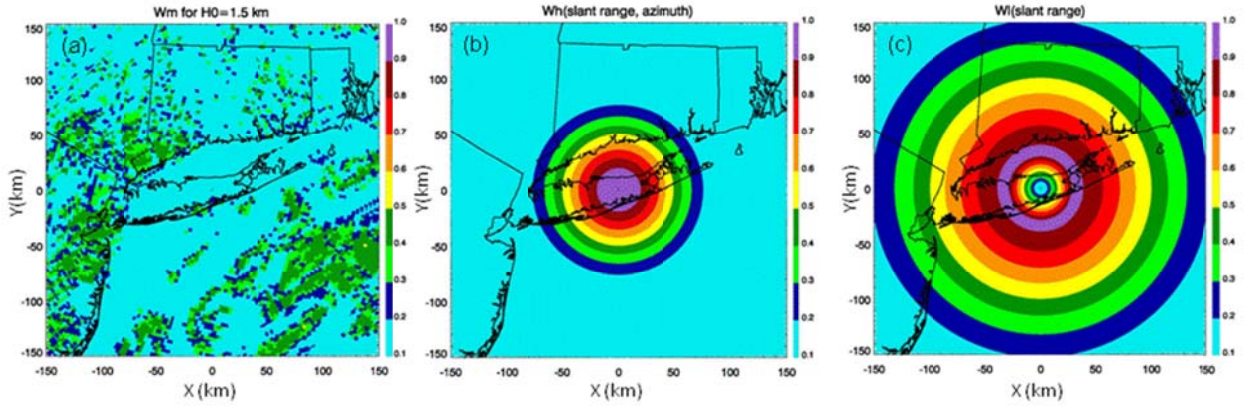

Figure 4: Weights derived from (a) equation (2) for the model-based ML detection, (b) equation (4) for the high-elevation radar-based detection, and (c) equation (3) for the low-elevation radar-based detection. The weight profiles are overlaid on a map of the NE U.S. centered on the KOKX WSR-88D radar (corresponding the radar fields displayed in Figure 3).

Figure 5 shows the 0.5º elevation locations where I_m=1, corresponding to where HRRR T_w on the 0.5º elevation surface falls between 0 and 4ºC, I_h=1, corresponding to where the range where *geometric projection* of the Ih detection heights fall on the 0.5º elevation surface, and I_l=1, corresponding to where the 0.5º elevation scan detects ML contribution using the methodology described by Krause et al. (2013). At this time, the high elevation radar-based ML detection of Giangrande et al. (2008), which often has to resort to sounding data in an insufficient number of ML detections were found at elevation anles between 4 and 10º, gave a ML_{BOT} and ML_{TOP} of ~2.0 and 2.5 km, respectively. The resulting geometric projection of those heights to the 0.5º elevation surface provides a ring of I_h=1, for this case, at a range where the corresponding W_h (Figure 4b) is so low that it would not be a significant contributor to overall ML product at the 0.5º elevation scan.

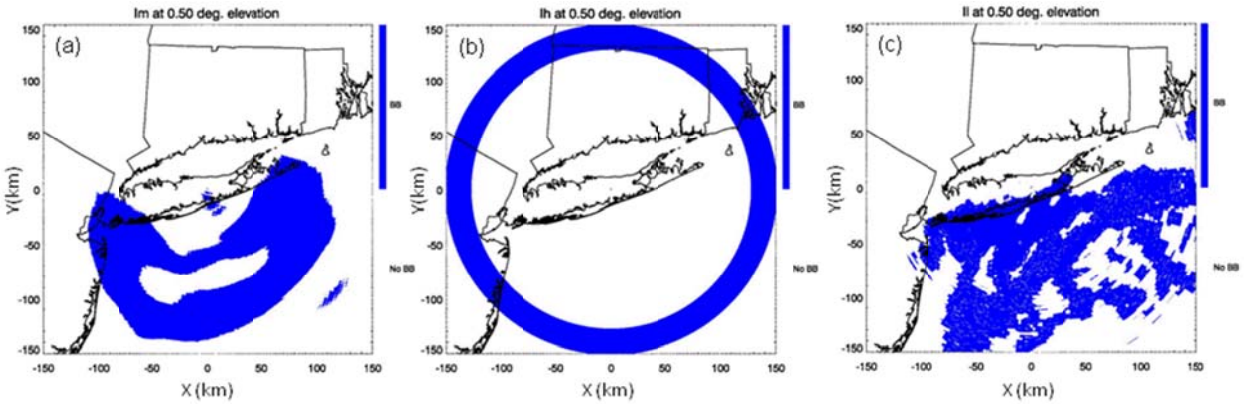

Figure 5: *Blue delineates the 0.5º elevation locations where (a) I_m=1, (b) I_h=1, and (c) I_l=1. The I_m, I_h, and I_l profiles are overlaid on a map of the NE U.S. centered on the KOKX WSR-88D radar (corresponding the radar fields displayed in Figure 3).*

Finally, we show Figures 6 and 7, which demonstrates the weighted product, A, given by equation (1) for the 0.5º elevation (Figure 6). Similar projections of A at other radar elevations < 4º are then combined into an "aggregated" surface projection of the maximum A (A_{surf}) at each location. Work in the near future will focus on optimizing the adaptable parameters and finding the threshold weight for A_{surf} that provides the most realistic solution.

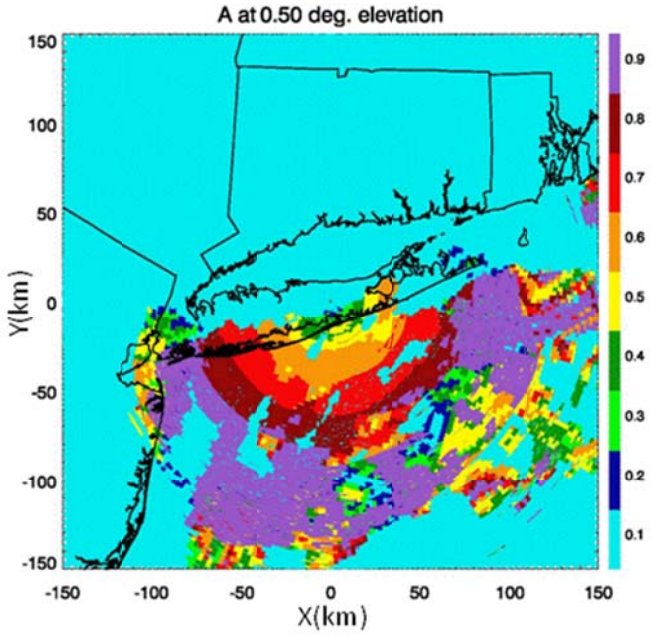

Figure 6: The value of A at 0.5º elevation derived from equation (1).

Summary and Future Work

In this paper, we have described the basic framework for a new "hybrid" ML detection algorithm that is designed to come up with an "optimal" ML solution by combining both radar- and model based techniques through the use of a methodology that attempts to take into account the advantages and disadvantages of each existing algorithm. Radar-based, range-dependent Gaussian weighting functions for both high- and low-elevation ML designations, which take into account inherent errors known to each technique, are combined with a model-based Gaussian weighting function that depends on horizontal gradients in wet-bulb temperatures to create a "blended" map of ML detections. A separate, time-dependent weighting function is used to account for time lag in the model analyses by de-emphasizing the contribution from the numerical model as the Δt from the radar volume and the most recent model analysis becomes large. A simple example of how the technique may be applied to a winter storm event is demonstrated on a radar volume collected by the polarimetric Upton, NY WSR-88D radar on 8 February 2013. Future work will focus on an extensive study of several events to determine 1) optimal values for the adaptable parameters, 2) the A_{surf} weight that gives the most realistic results.

Acknowledgement

Funding was provided by NOAA/Office of Oceanic and Atmospheric Research under NOAA-University of Oklahoma Cooperative Agreement #NA11OAR4320072, U.S. Department of Commerce, and by the U.S. National Weather Service, Federal Aviation Administration, and Department of Defense program for modernization of NEXRAD radars.

References

Giangrande, S. E., J. M. Krause, and A. V. Ryzhkov, 2008: Automated designation of the melting layer with a polarimetric prototype of the WSR-88D radar. *J. Appl. Meteor. Climatol.,* **47**, 1354-1364.

Krause, J., V. Lakshmanan, and A. Ryzhkov, 2013: Improving detection of the melting layer using dual-polarization radar, NWP model data, and object identification techniques. *36th Conference on Radar Meteorology*, Breckenridge, CO, American Meteorological Society, Boston, 262.

Park, H.-S., A. V. Ryzhkov, D. S. Zrnic, and K-.E. Kim, 2009: The hydrometeor classification algorithm for the polarimetric WSR-88D: Description and application to an MCS. *Wea. Forecasting*. 24, 730-748.

Schuur, T. J., Park, H.- S., A. V. Ryzhkov, and H. D. Reeves, 2012: Classification of precipitation types during transitional winter weather using the RUC model and polarimetric radar retrievals. *J. Appl. Meteor. Climate*, 51, 763-779. DOI: 10.1175/JAMC-D-11-091.1.

Schuur, T. J., A. V. Ryzhkov, H. D. Reeves, J. Krause, K. L. Elmore, and K. L. Ortega, 2014: Recent modifications to a new surface-based polarimetric Hydrometeor Classification Algorithm for the WSR-88D network, *8th European Conference on Radar in Meteorology and Hydrology*, Garmisch-Partenkirchen, Germany, 7.5.

Giangrande, S. E., J. M. Krause, and A. V. Ryzhkov, 2008: Automated designation of the melting layer with a polarimetric prototype of the WSR-88D radar. *J. Appl. Meteor. Climatol.,* **47**, 1354-1364.